ACS OMEGA

Article

Cite This: ACS Omega 2019, 4, 3306−3313

http://pubs.acs.org/journal/acsodf

Unimolecular Decomposition Reactions of Propylamine and Protonated Propylamine

Mansour H. Almatarneh,*[,†,‡] Ismael A. Elayan,[†] Mazen Al-Sulaibi,[†] Ahmad Al Khawaldeh,[†] Sedeeqa O. W. Saber, Mahmood Al-Qaralleh,[†] and Mohammednoor Altarawneh[§,∥]

[†]Department of Chemistry, University of Jordan, Amman 11942, Jordan

[‡]Chemistry Department, Memorial University, St. John's, Newfoundland and Labrador A1B 3X7, Canada

[§]School of Engineering and Information Technology, Murdoch University, 90 South Street, Murdoch, Western Australia 6150, Australia

[∥]Chemical Engineering Department, Al-Hussein Bin Talal University, Ma'an 71111, Jordan

Supporting Information

ABSTRACT: A detailed computational study of the decomposition reaction mechanisms of *cis*-propylamine (*cis*-PA), *trans*-propylamine (*trans*-PA), and the cis-isomer of its protonated form (*cis*-HPA) has been carried out. Fourteen major pathways with their kinetic and thermodynamic parameters are reported. All reported reactions have been located with a concerted transition state, leading to significant products that agree with previous theoretical and experimental studies. Among six decomposition pathways of *trans*-PA, the formation of propene and NH_3 is the significant one, kinetically and thermodynamically, with an activation energy barrier of 281 kJ mol^{-1}. The production of two carbenes is found via two different transition states, where the reactions are thermodynamically controlled and reversible. Furthermore, five decomposition pathways of *cis*-PA have been considered where the formation of ethene, methylimine, and H_2 is the most plausible one with an activation energy barrier of 334 kJ mol^{-1}. The results show that the formation of propene and NH_4^+ from the decomposition of *cis*-HPA is the most favorable reaction with an activation barrier of 184 kJ mol^{-1}, that is, the lowest activation energy calculated for all decomposition pathways.

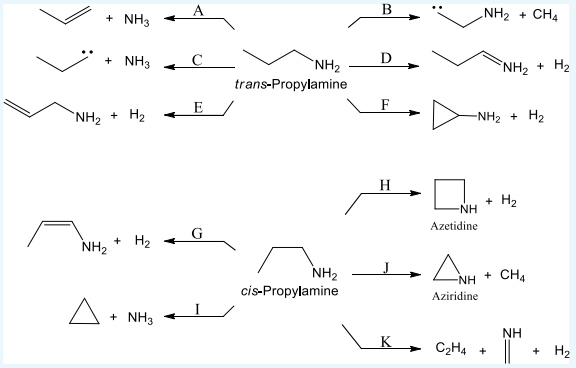

INTRODUCTION

n-Propylamine (PA) is an aliphatic primary amine with the chemical formula C_3H_9N. PA is incessantly included in organic syntheses, industrial formulation, and biological processes. In pharmacopeia, PA used as a synthetic precursor for antifungal,[1] antimalarial,[2] antibacterial,[3] antivirals,[4] and anticancer[5] agents. In the processing of nanomaterials, PA is utilized in the synthesis,[6,7] size[8] and morphology[9] control, and functionalization of nanosized products.[10] Moreover, PA found applications in the preparation of catalysts,[11−13] molecular sieves,[14] corrosion inhibitors,[15,16] and removal of liquid[17] and gaseous[18] pollutants. The combustion of PA with fuels leads to the formation of nitrogenized pollutants, that is, HCN, HCNO, and NH_3.[19,20] These pollutants, if emitted, react with carbonyl oxide (Criegee intermediate) and contribute to the secondary organic aerosol formation, thus contributing to climate change.[21] The widespread applications of PA raise the environmental concern about the emitted species during environmental remediation of PA-containing products.

The decomposition of both PA and protonated *n*-propylamine (HPA) has been the focus of several studies.[22−26] The decomposition of PA shows significant chemical characteristics that require further investigation. The reaction is homogeneous and apparently unimolecular;[26] furthermore, it is the first order and probably a chain one.[27] The order of skeletal bond scission probability is α-CC bond > CN bond > β-CC bond.[28] PA has a peculiar property in that it dissociatively ionize with the production of alkyl-free radicals in addition to methylenimmonium ion $CH_2NH_2^+$[29] which is considerably stabilized by the formation of C═N π-bond,[30] whereas the NH_3 loss, that is analogous to the dehydration of *n*-propylalcohol, is unfavorable[31] due to the electrostatic repulsion between the terminal heavy atoms.[32] In the presence of kaolin,[33] the PA is decomposed into hydrogen cyanide (6.6%), propylene (6.4%), H_2 (6.3%), N_2 (4.6%), and ethylene (3.0%). On the silicon Si surface, eight decomposition products were studied theoretically.[25] The formation π-bond-containing products, alkyl cyanide (activation energy 242 kJ mol^{-1}), alkene (334 kJ mol^{-1}), and imine(343 kJ mol^{-1}), were the most plausible dissociation pathways, whereas the

Received: October 13, 2018
Accepted: January 31, 2019
Published: February 14, 2019

DOI: 10.1021/acsomega.8b02792
ACS Omega 2019, 4, 3306−3313

formation of strained cyclic products, azetidine (467 kJ mol^{-1}), cyclopropane (493 kJ mol^{-1}), and aziridine (506 kJ mol^{-1}), were kinetically less favorable. The formation of NH_3 and H_2 is within acceptable activation energy values of 384 and 400 kJ mol^{-1}, respectively.[25] In aqueous solution, the PA is in equilibrium with HPA. The proton affinity and the structural change of PA through protonation affect the dissociation products of HPA.[34,35] Experimental studies showed that it follows three fragmentation patterns corresponding to propene loss, NH_3 loss, and ethane elimination.[22,24]

There are different experimental factors that affect the fragmentation pattern of amines, including the activation or fragmentation regime,[36] the applied power and time, the internal energies of the molecular ions,[37] and the molecular weight.[38] Collectively, these factors account for the experimental inconsistency in the reported products, fragmentation patterns, and intensities. Hence, further understanding is required on the decomposition reactions of PA (Scheme 1)

Scheme 1. Proposed Decomposition Reactions of *trans*-PA and *cis*-PA

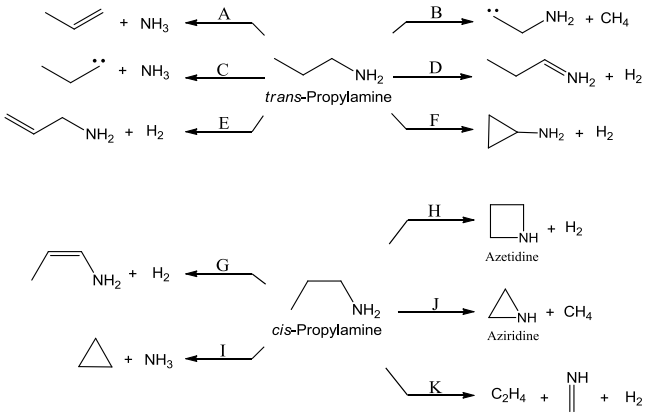

Scheme 2. Proposed Decomposition Reactions of *cis*-HPA

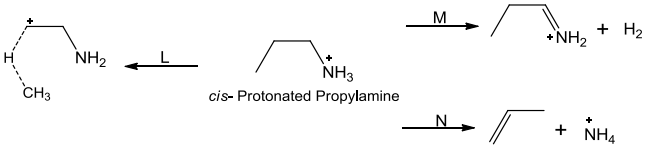

and HPA (Scheme 2). This shall shed more light on the chemistry of the decomposition reactions, formed products, and decrease the uncertainties in the previous literature. Therefore, the goal of this computational study is to further investigate and study novel pathways of the dissociation of PA and HPA. Furthermore, the formed products through different pathways are compared with the reported experimental data to ensure the results of this work.

RESULTS AND DISCUSSION

Different gas-phase decomposition pathways of PA have been studied to provide more kinetic and mechanistic insights. The studied pathways are based on previous experimental findings[26,27] and further computational consideration is built on chemical intuition and different discoveries. It is worth noting that all studied decomposition pathways occur in a concerted step as an endothermic process. The kinetic parameters (E_a, $\Delta H^{\ddagger}$, and $\Delta G^{\ddagger}$) for the investigated pathways are reported herein at different levels of theory. The plausible pathways that will be discussed are compared based on the calculated kinetics, the lower the energy the more plausible the reaction. The reaction coordinates (R: reactant, **TS**: transition state, and P: product) are depicted on a potential energy surface (PES) for related pathways to define the energies of the most plausible pathways. The α-, β-, and γ-carbons of PA with respect to the nitrogen atom are indicated in some pathways, upon discussion, whenever is needed.

Decomposition of *trans*-Propylamine. The cis and trans are conformational isomers; however, both isomers lead to the formation of different products. A connection between both isomers through the same pathways has been accounted for; however, the energy barrier is very negligible. For example, the experimentally detected cyclic forms of aziridine, azetidine, and cyclopropane are produced from the cis-isomer while other forms are produced more easily from the trans. The decomposition of *trans*-propylamine (*trans*-PA) leads to the formation of different products of propene, carbene ($CH_3CH_2\ddot{C}H$), imine, cyclopropanamine, NH_3, H_2, and CH_4. This section examines the formation of these products through six separate pathways (see Scheme 1 and Figure 1).

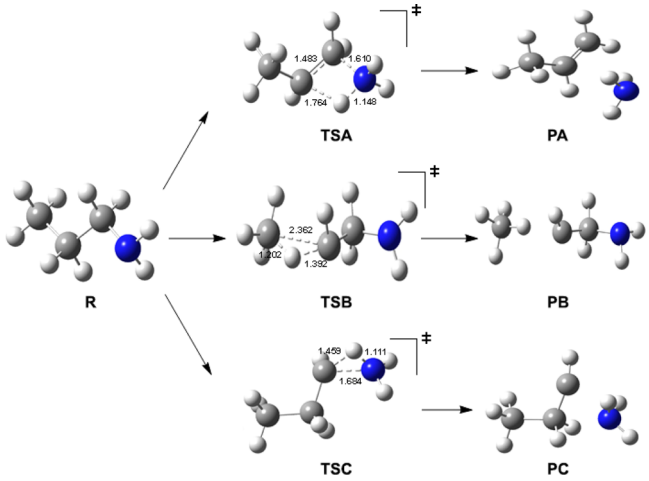

Figure 1. Proposed reaction mechanisms for the decomposition of *trans*-PA (pathways **A** to **C**).

One of the most indicated and proposed pathways in the decomposition reactions is the formation of an alkene and NH_3. Herein, this route of reaction is designated as pathway **A**, where **TSA** shows how the C−N and C−H bonds are elongated to 1.610 and 1.764 Å, respectively, while the C−C bond length is decreased to 1.483 Å. This dissociation step is a concerted one step that leads to the formation of propene and NH_3 (**PA**), see Figure 1. The activation energy of **TSA** is lower compared to other pathways with a value of 297 kJ mol^{-1} at B3LYP/6-31G(d). Increasing the Gaussian functions to B3LYP/6-311++G(3df,3pd) decreased the energy barrier to 283 kJ mol^{-1}, that is, in agreement with the lower calculated value of 281 kJ mol^{-1}, at CBS-QB3. The thermodynamic parameters indicate that the reaction is endothermic by 39 kJ mol^{-1} and endergonic by 16 kJ mol^{-1} at CBS-QB3. The calculated activation energies are given in Table 1 at different levels of theory.

DOI: 10.1021/acsomega.8b02792
ACS Omega 2019, 4, 3306−3313

Table 1. Kinetic Parameters (E_a, $\Delta H^{\ddagger}$, and $\Delta G^{\ddagger}$) for the Decomposition of *trans*-PA (in kJ mol^{-1}) at 298.15 K

	levels of theory								
	B3LYP/6-31G(d)			B3LYP/6-311++G(3df,3pd)			CBS-QB3		
pathways (**TS**)	$E_{a(0K)}$	$\Delta H^{\ddagger}$	$\Delta G^{\ddagger}$	$E_{a(0K)}$	$\Delta H^{\ddagger}$	$\Delta G^{\ddagger}$	$E_{a(0K)}$	$\Delta H^{\ddagger}$	$\Delta G^{\ddagger}$
pathway A (**TSA**)	297	298	296	283	283	282	281	281	280
pathway B (**TSB**)	404	406	399	388	390	383	391	393	387
pathway C (**TSC**)	349	351	346	330	332	328	329	331	327
pathway D (**TSD**)	395	396	396	379	379	379	379	380	380
pathway E (**TSE**)	424	426	423	393	396	392	401	404	400
pathway F (**TSF**)	420	420	421	401	400	401	406	405	406

Another significant route is producing CH_4, which can be generated through two different reaction mechanisms. For example, pathway **B** occurs from the *trans*-PA while another different mechanism of pathway **J** (discussed in a further section) is initiated from the *cis*-propylamine (*cis*-PA), generating different coproducts. Pathway **B** involves the dissociation of the terminal γ-carbon through **TSB** with a bond length of 2.362 Å from the β-carbon, followed with a simultaneous proton transfer with a length of 1.202 and 1.392 Å approaching the γ and away from the β-carbon, respectively (Figure 1). Interestingly, this step produces a carbene ($\ddot{C}HCH_2NH_2$) and CH_4 as final products (**PB**). However, compared to pathways **B** and **C**, the reaction is not kinetically favored because of the high calculated energy barriers of 404 kJ mol^{-1} at B3LYP/6-31G(d), 388 kJ mol^{-1} at B3LYP/6-311++G(3df,3pd), and 391 kJ mol^{-1} at CBS-QB3. The high energy barrier could be attributed to the formation of the carbene where the carbon is sp-hybridized. However, the lower activation energy values of **TSC** via pathway **C** mark that this is not the main case because another carbene of $CH_3CH_2\ddot{C}H$ with NH_3 as a coproduct (**PC**) is formed with respective values of 349, 330, and 329 kJ mol^{-1} at B3LYP/6-31G(d), B3LYP/6-311++G(3df,3pd), and CBS-QB3, respectively (Table 1). The carbene in pathway **C** is formed through the detachment of the C−N bond length of 1.684 Å with a simultaneous proton transfer from the α-carbon of 1.459 Å to the amino group forming **PC**. It is worth noting that based on the PES of Figure 3, pathways **B** and **C** are thermodynamically reversible. The carbenes most probably will react with other species in the atmosphere as they are very reactive and unstable.

The formation of an imine and H_2 (pathway **D**) through the decomposition of *trans*-PA via **TSD** occurs with a single step by the removal of H_2 from PA with lengths of 1.560 and 1.437 Å. Simultaneously, the C═N imine bond is formed where the C−N bond decreased by about 0.8 Å to become 1.387 Å, see Figure 2. Likewise, pathway **E** signifies the formation of prop-2-en-1-amine and H_2 (**PE**) through **TSE**. However, the kinetic scenario is different in favorability where the former (**TSD**) is more favorable than the latter (**TSE**) at different levels of theory. The activation energy values for **TSD** are lower than **TSE** by 29, 14, and 22 kJ mol^{-1} at B3LYP/6-31G(d), B3LYP/6-311++G(3df,3pd), and CBS-QB3, respectively. Moreover, enthalpies and Gibbs energies of activation are lower, significantly favoring pathway **D** than **E**, refer to Table1. Furthermore, thermodynamically, pathway **D** is more favorable with lower parameters (ΔE, ΔH, and ΔG) and by 71 kJ mol^{-1}.

Ultimately, the formation of cyclopropanamine and H_2 through a different decomposition route, pathway **F**, undergoes **TSF** in a cyclization step. C−C bond with a length of 2.577 Å and hydrogens secession from the α- and γ-carbons of 2.735 and 2.109 Å, respectively. The hydrogen attached to the α-carbon is distinct from the γ with a length longer by about 0.6 Å, and this is attributed to its C−N bond that leads to a higher steric factor. However, in terms of energy, this reaction mechanism and formed products (**PF**) are not kinetically favored. Table 1 shows that for pathways **F** and **E** (producing H_2), the activation energies are higher than the other investigated pathways at different levels of theory. For instance, the calculated energy barrier for the **TSF** value of 406 kJ mol^{-1} at CBS-QB3 is the highest among the other transition state energies. Interestingly, the thermodynamic calculations of this reaction mechanism are more favored than the other *trans*-PA H_2-producing pathways **D** and **E**. The respective enthalpy and Gibbs energy values of 83 and 65 kJ mol^{-1} are more favored than for pathways **D** and **E** by about 7 and 74 kJ mol^{-1}, respectively. This result sheds more light on the mechanism of how H_2 is produced more favorably through pathway **D** and further helps in explaining why the cyclopropanamine and propenamine are not experimentally detected. The relative energies of a PES for the investigated decomposition pathways of *trans*-PA are given in Figure 3. It is worth noting that increasing the polarization and diffuse functions at B3LYP/6-311++G(3df,3pd) decreased the energies of all pathways, and the calculated energies for all TSs are consistent to CBS-QB3 by no more than 5 kJ mol^{-1} difference.

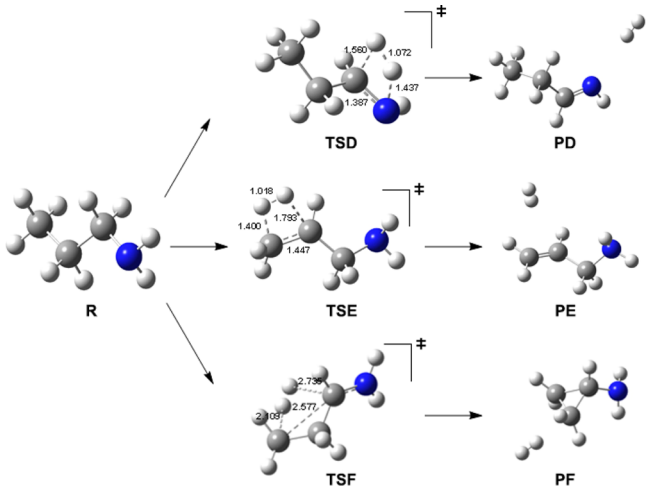

Figure 2. Proposed reaction mechanisms for the decomposition of *trans*-PA (pathways **D** to **F**).

Decomposition of *cis*-PA. The decomposition of *cis*-PA, as other separate pathways occur, is due to the geometry of the PA; in which the *trans*-PA cannot undergo these reaction mechanisms and vice versa. Furthermore, the decomposition from both stereoisomers to form H_2 proves that the yield of

DOI: 10.1021/acsomega.8b02792
ACS Omega 2019, 4, 3306−3313

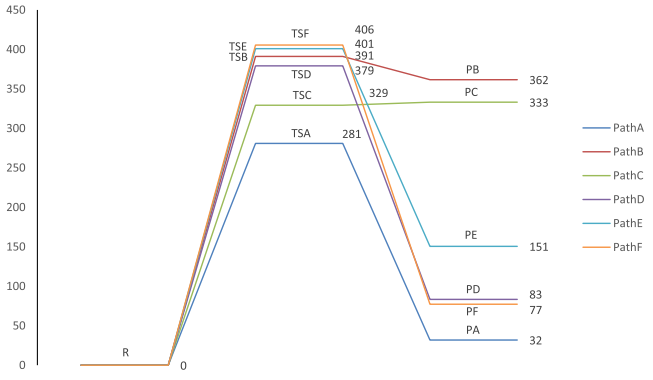

Figure 3. PES of the decomposition of *trans*-PA, pathways **A** to **F**, calculated at CBS-QB3.

6.3% cannot be neglected and might be more than expected.[33] For example, **TSG** through pathway **G** is a different one that leads to the formation of prop-1-en-1-amine and H_2 (similar to pathway **E** but with geometric isomerism). However, bond lengths and activation energies of **TSG** differ from **TSE**; this is attributed to the terminal alkene that is being formed in **TSE** which is less sterically hindered than **TSG**. The hydrogens dissociate from the α and γ-carbons with lengths of 2.445 and 1.186 Å with a forming C═C double bond of 1.448 Å, see Figure 4.

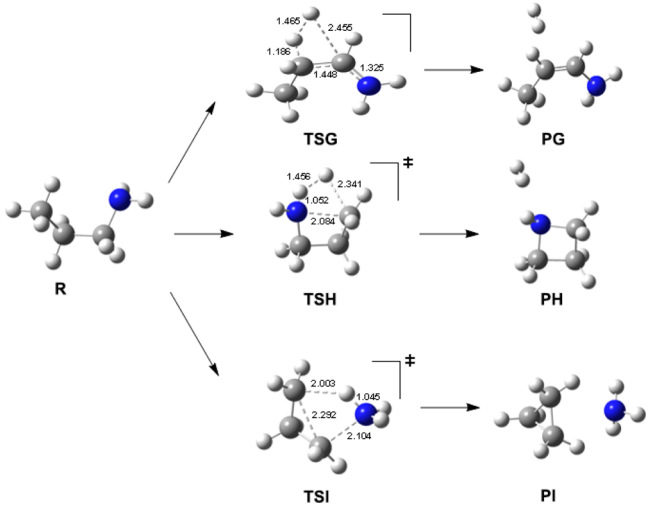

Figure 4. Proposed reaction mechanisms for the decomposition of *cis*-PA (pathways **G**, **H**, and **I**).

The more favorable formation of **TSE** rather than **TSG** is also confirmed through the activation energies, where it is higher in the latter by about 88 kJ mol^{-1}at different levels of theory (Table 2). The activation energy value of 499 kJ mol^{-1} at B3LYP/6-31G(d) decreased to 481 kJ mol^{-1} at B3LYP/6-311++G(3df,3pd). Moreover, the calculations at CBS-QB3 are in agreement with both levels with a value of 489 kJ mol^{-1}. However, it is worth noting that thermodynamically, pathway **G** is more plausible with lower enthalpy and Gibbs energies by about 34 and 40 kJ mol^{-1} at different levels of theory.

As for the cyclic products, three significant pathways (**H**, **I**, and **J**) with different transition states were determined. Pathway **H**, where *cis*-PA decomposes to azetidine and H_2 (PH), undergoes a reaction mechanism of C−N bond formation of 2.084 Å and H_2 dissociation from the nitrogen atom and γ-carbon of 1.052 and 2.341 Å, respectively. However, the barrier heights of 500, 494, and 492 kJ mol^{-1} (Table 2) are higher than the previously reported value of 467 kJ mol^{-1}, and this referred to the fact that Cho and Choi[25] studied the decomposition pathways on a silicon surface. It should be noted that the cyclic formation pathways are indicated here according to their relevance. Moreover, in order to avoid repetition, the more plausible transition states are purely described while other ones are indicated by comparison and relevance.

Although the cyclopropane is more hindered than azetidine, it is found to be more favored in terms of energies, where the **TSI** barrier is lower than **TSH**, see Table 2. Furthermore, it is more thermodynamically favored with lower energies by about 100 kJ mol^{-1} at the reported levels. Thus, the presence of a nitrogen atom in **PH** alters the chemical reaction of electron delocalization from **PI**, which is also confirmed from the decomposition to aziridine and CH_4 through **TSJ** (pathway **J**), see Figure 5. This indicates that **TSJ** is more plausible than **TSH**; hence, pathway **J** is more favored kinetically and thermodynamically than **H**.

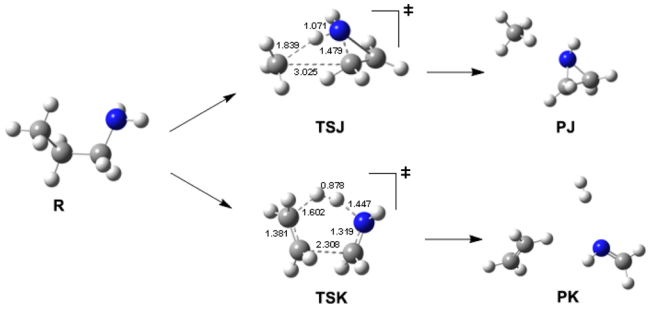

Figure 5. Proposed reaction mechanisms for the decomposition of *cis*-PA (pathways **J** and **K**).

The more favored **TSI** forms the cyclopropane and NH_3 (**PI**) through the dissociation of the amino group from the α-carbon of 2.104 Å with simultaneous proton transfer from the

Table 2. Kinetic Parameters (E_a, $\Delta H^{\ddagger}$, and $\Delta G^{=\ddagger}$) for the Decomposition of *cis*-PA (in kJ mol^{-1}) at 298.15 K

	levels of theory								
	B3LYP/6-31G(d)			B3LYP/6-311++G(3df,3pd)			CBS-QB3		
pathways (**TS**)	$E_{a(0K)}$	$\Delta H^{\ddagger}$	$\Delta G^{\ddagger}$	$E_{a(0K)}$	$\Delta H^{\ddagger}$	$\Delta G^{\ddagger}$	$E_{a(0K)}$	$\Delta_H{}^{\ddagger}$	$\Delta G^{\ddagger}$
pathway G (**TSG**)	499	501	498	481	482	480	489	490	487
pathway H (**TSH**)	500	498	503	494	492	496	492	490	494
pathway I (**TSI**)	435	436	434	414	416	413	416	417	414
pathway J (**TSJ**)	479	481	476	459	462	455	466	469	463
pathway K (**TSK**)	343	343	343	333	333	334	334	333	334

DOI: 10.1021/acsomega.8b02792
ACS Omega 2019, 4, 3306−3313

γ-carbon of 2.003 Å. This is accompanied by a C−C bond formation of 2.292 Å, corresponding to the cyclopropane formation, through **TSI**, with an activation energy of 435 kJ mol^{-1} at B3LYP/6-31G(d). The calculated results at B3LYP/6-311++G(3df,3pd) and CBS-QB3 levels of theory are consistent with energy barriers of 414 and 416 kJ mol^{-1}, respectively. Furthermore, Table 2 shows that the energy values of decomposition to aziridine with CH_4 (**TSJ**, Figure 5) and cyclopropane with NH_3 (**TSI**) are lower than the previously reported values[25] of 506 and 493 kJ mol^{-1}, respectively.

The calculated activation energies of **TSI** are lower than **TSH** and **TSJ**, see Table 2. Thus, among the cyclic formation pathway, pathway **I** is the most plausible one. However, this does not mean that the other products are not formed because the decomposition reactions occur at very high temperatures that aid in the formation of different unexpected products. Moreover, studying the decomposition reaction and its modeling on other cluster surfaces increases the expectation of forming other products by acting as a catalyst surface for these reactions, considering the fact that also some products undergo further unimolecular or bimolecular reactions, leading to the formation of other products.

An interesting novel decomposition reaction, pathway **K**, that leads to the formation of ethane, methanimine, and H_2 is found to be kinetically more favored than other pathways. The reaction parameters shown in Figure 5 depict the concerted step, **TSK**, of C−C and H_2 dissociation. The former belongs to an α- and β-carbon length of 2.308 Å, while the latter belongs to 1.447 and 1.602 Å from the nitrogen and γ-carbon, respectively. This change in bond lengths is accompanied by the formation of imine with 1.319 Å and C═C double bond of 1.381 Å (**PK**). Extensive efforts to find a step-wise mechanism of this reaction to check with the bond lengths and energy barriers were considered; however, all efforts lead to the concerted one. It should be noted that the product geometries of pathway **K** are obtained at B3LYP/6-31G(d) because we were unable to locate the final products (**PK**) at B3LYP/6-311++G(3df,3pd) and CBS-QB3 levels of theory.

The kinetic scenario fulfills a reputable reaction barrier of the investigated decomposition reaction of *cis*-PA, where the calculated activation energies are the lowest compared to other pathways, see Table 2. The activation energy value of 343 kJ mol^{-1} at B3LYP/6-31G(d) is lower than range off other pathways and further improvement of basis sets conformable to the B3LYP/6-311++G(3df,3pd) level of theory decreased the barrier by 10 kJ mol^{-1}. This value is also consistent with CBS-QB3 calculated energy barrier value of 334 kJ mol^{-1}. Thus, pathway **K** is considered the most plausible pathway with lower activation energies at different levels of theory. This is also given in Figure 6 as a comparative PES of the investigated pathways at CBS-QB3. This reaction mechanism may also be the indicated sink reaction for the formation of H_2 because it has a yield of 6.3%, along with the experimentally detected ethylene with its yield of 3.0%.[36] This also shows the probabilities of H_2 and other product formation through different decomposition reactions. It should be noted here that the barriers at B3LYP/6-311++G(3df,3pd) are comparable to CBS-QB3, differing by no more than 8 kJ mol^{-1}.

Decomposition of *cis*-HPA. The selection of the cis-isomerism of HPA rather than the trans is based on the investigated pathways (**L**, **M**, and **N**), in which it is possible to locate the desired transition states and products from the cis.

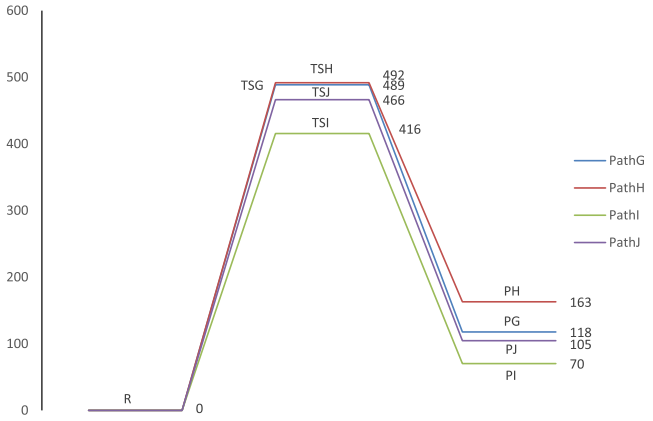

Figure 6. PES of the decomposition of *cis*-PA, pathways **G** to **J**, calculated at CBS-QB3.

This is based on our efforts to locate other transition states to find other pathways from the trans-isomer, which all leads to the investigated pathways of **L**, **M**, and **N**. The protonation is on the amino group (NH_2) of PA that leads to the formation of an ammonia (NH_3^+) group, that is, a significant moiety for proton-related reactions as it will be discussed in this section.

The momentum of the ammonia group (NH_3^+) of HPA is proton releasing to α-, β-, or γ-carbons, which results in different kinetics, thermodynamics, and bond parameters. Pathway **L** shows the proton transfer from $NH_3^+$to γ-carbon with a length of 1.816 Å, followed by a simultaneous proton transfer of 1.553 Å from the γ- to β-carbon via **TSL**, see Figure 7. Interestingly, this step led to the formation of a hydrogen

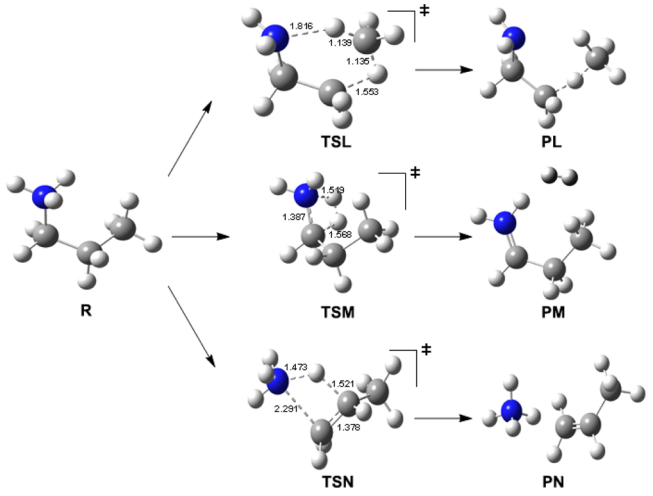

Figure 7. Proposed reaction mechanisms for the decomposition of *cis*-PA (pathways **G**, **H**, and **I**).

bond bridge between the β- and γ-carbons (**PL**), where the positive charge is located on the CH_2 group (as shown in Scheme 2). Despite our extensive efforts, we were unable to locate a **TS** of the dissociation of the hydrogen bound complex that produces the desired products. Therefore, we believe that, at this state, the reaction proceeds to the hydrogen bound complex (the located product on the PES) with a higher energy barrier which makes it a kinetically unfavorable step and it is not worth investigating more. On the other hand, the barrier heights for **TSL** are relatively lower than the investigated decomposition pathways of *cis*- and *trans*-PA,

DOI: 10.1021/acsomega.8b02792
ACS Omega 2019, 4, 3306−3313

Table 3. Kinetic Parameters (E_a, $\Delta H^{\ddagger}$, and $\Delta G^{\ddagger}$) for the Decomposition of *cis*-HPA (in kJ mol^{-1}) at 298.15 K

	levels of theory								
	B3LYP/6-31G(d)			B3LYP/6-311++G(3df,3pd)			CBS-QB3		
pathways (**TS**)	$E_{a(0K)}$	$\Delta H^{\ddagger}$	$\Delta G^{\ddagger}$	$E_{a(0K)}$	$\Delta H^{\ddagger}$	$\Delta G^{\ddagger}$	$E_{a(0K)}$	$\Delta H^{\ddagger}$	$\Delta G^{\ddagger}$
pathway L (**TSL**)	277	277	278	265	265	266	269	269	270
pathway M (**TSM**)	332	334	329	311	314	309	317	320	315
pathway N (**TSN**)	197	201	191	181	185	174	184	188	178

where the barriers are 277, 265, and 269 kJ mol^{-1} at the B3LYP/6-31G(d), B3LYP/6-311++G(3df,3pd), and CBS-QB3 levels of theory (Table 3), respectively, particularly because these energies are significantly lower than other CH_4-forming pathways of **B** and **J** by about 197 kJ mol^{-1}. However, for pathway **L**, the PES in Figure 8 shows that the reaction is thermodynamically reversible with low product energies relative to the transition states.

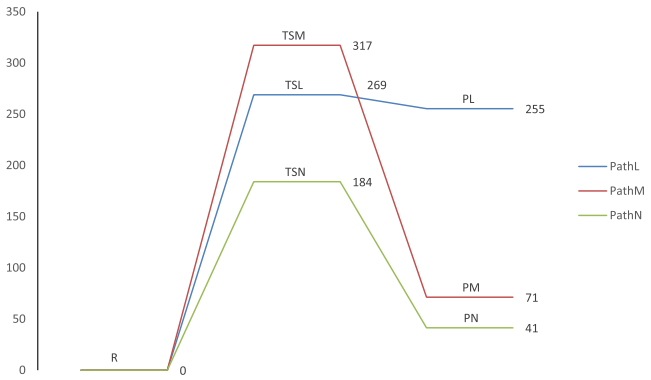

Figure 8. PES of the decomposition of *cis*-HPA and pathways **L**, **M**, and **N**, calculated at CBS-QB3.

As mentioned earlier, there are considerable pathways of H_2 production. For example, pathway **M** describes the formation of H_2 through dissociation of the hydrogen bonds from the NH_3^+ and β-carbon with bond lengths in the range of 1.519 Å through **TSM** (Figure 7). Furthermore, this step of **TSM** leads to the formation of protonated propanimine (**PM**) with an imine consistent with other pathway bond length of 1.387 Å. However, the calculated energy barrier of **TSM** is exceedingly high, in comparison to other steps, with a value of 332 kJ mol^{-1}, at B3LYP/6-31G(d). Further calculations at B3LYP/6-311++G(3df,3pd) and CBS-QB3 lower the energy barriers to 311 and 317 kJ mol^{-1} (Table 3), respectively. Relative energies of this pathway compared to other ones are given in a PES of Figure 8, where the reaction is endothermic and exergonic by 77 kJ mol^{-1}.

Essentially, the production of ammonium cation (NH_4^+) along with propene is the most anticipated reaction mechanism of *cis*-HPA because of the presence of the galvanizing nitrogen moiety toward having the additional hydrogen. The reaction is initialized via **TSN** by the nitrogen dissociation followed with the hydrogen abstraction from the β-carbon with bond lengths of 2.291 and 1.521 Å, see Figure 8. The latter bond (N−H) formation has a bond length of 1.473 Å, that is, higher than the other N−H bond formation by about 0.4 Å. Furthermore, this concerted step is accompanied with the C=C double-bond formation with a bond length of 1.378 Å. The reaction is considerable with the lowest activation energies of all investigated pathways, making **TSN** the most plausible transition structure with an activation energy of 197 kJ mol^{-1} at B3LYP/6-31G(d). Further addition of polarization and diffuse functions led to a decrease in the energy barrier by 16 kJ mol^{-1}. This is in agreement with the complete basis set method, CBS-QB3, the value of 184 kJ mol^{-1}, refer to Table 3. Thus, based on the calculated energies and relative to other pathways (Figure 8), the reaction is kinetically favored and the most plausible pathway, forming propene and NH_4^+ (**PN**). It should be mentioned that the barriers at B3LYP/6-311++G(3df,3pd) are comparable to CBS-QB3 differing by no more than 6 kJ mol^{-1}.

CONCLUSIONS

A thorough computational study of the gas-phase decomposition of PA and its protonated form has been detailed using density functional theory (DFT) and CBS-QB3 methods. Fourteen different pathways have been investigated; six for *trans*-PA, five for the *cis*-PA, and three for the *cis*-HPA. The kinetic and thermodynamic parameters have been reported at different levels of theory. Each desired reactant, transition structure, and product have been optimized and ensured its connection to the related pathway at different levels of theory. Two pathways have been considered to lead to the carbine formation with different reaction energies. Different decomposition pathways that lead to the formation of H_2 along with significant products of propene, CH_4, NH_4^+, and imine have been studied, compared, and reported, kinetically and thermodynamically. The most favored (energetically) pathways in the investigated decomposition reactions are **A** (281 kJ mol^{-1}), **K** (334 kJ mol^{-1}), and **N** (184 kJ mol^{-1}) of *trans*-PA, *cis*-PA, and *cis*-HPA, respectively. Furthermore, three different pathways (**B**, **C**, and **L**) with thermodynamic reversibility were located and studied. Further unimolecular and bimolecular reactions are expected to occur and affect the energy barrier of the decomposition of PA, along with the need for further understanding of HPA decomposition chemistry because it leads to different products.

Computational Methods. All of the electronic structure calculations have been considered using the Gaussian 09 quantum package.[39] Geometries were initially optimized by employing the hybrid method of Becke's three-parameter using the LYP functional (B3LYP),[40,41] utilizing the 6-31G(d) basis set.[42] Further calculations by increasing the Gaussian functions corresponding to B3LYP/6-311++G(3df,3pd) were considered; this is to test the effects of polarization and diffuse functions on the energy barrier and ensure the reliability of calculations. Moreover, single-point energy calculations were employed using the more accurate method, CBS-QB3.[43] The selected methods are also based on our previous studies of the decomposition pathways of different amines.[19,44−47]

Minimum energy stationary points were located and defined by first optimizing the geometries of the minima and saddle points. Analysis of the harmonic vibrational frequency of

DOI: 10.1021/acsomega.8b02792
ACS Omega 2019, 4, 3306−3313

minima showed no imaginary frequency, while the transition state shows only one negative imaginary frequency in the Hessian matrix for the desired reaction pathways. Further analysis of transition states via the intrinsic reaction coordinate[48] at B3LYP/6-31G(d) ensured the connection of the desired points for each proposed mechanism. Each reaction pathway is depicted on the PES along with the reacting points. The PES formulates the calculated activation energies relative to the initial reactive complex, which draws more conclusions on the investigated reaction pathways. All relative energies of optimized geometries were corrected with zero-point vibrational energies. The calculated activation energies (E_a) are reported at 0 K, while enthalpies of activation ($\Delta H^{\ddagger}$) and Gibbs energies of activation ($\Delta G^{\ddagger}$) are at 298.15 K.

B3LYP/6-31G(d) is the most commonly used functional, however, it still misses the long-range dispersion effect and van der Waals interactions. Furthermore, the accurate prediction of energy barriers, as well as the kinetics, is still a challenge to the B3LYP functional and DFT methods. Hence, the utilization of the composite method, CBS-QB3, comes in handy; due to the accurate description of energy barriers. Increasing the Gaussian functionals, corresponding to B3LYP/6-311++G(3df,3pd), produces energy values in qualitative agreement with the CBS-QB3 calculations, within no more than 8 kJ mol^{-1}. This indicates that the B3LYP/6-311++G(3df,3pd) level of theory performs well to this system; however, further and different functionals should be used in future studies to describe the pyrolysis/decomposition reactions.

■ ASSOCIATED CONTENT

Supporting Information

The Supporting Information is available free of charge on the ACS Publications website at DOI: 10.1021/acsomega.8b02792.

Cartesian coordinates of all optimized geometries for all proposed mechanisms along with the vibrational frequencies (PDF)

■ AUTHOR INFORMATION

Corresponding Author

*E-mail: m.almatarneh@ju.edu.jo. Phone: (+962) 65355000-Ext. 22162.

ORCID

Mansour H. Almatarneh: 0000-0002-2863-6487

Mohammednoor Altarawneh: 0000-0002-2832-3886

Notes

The authors declare no competing financial interest.

■ ACKNOWLEDGMENTS

We are gratefully acknowledge the Atlantic Computational Excellence Network (ACENET) and Compute Canada for the computer time.

■ REFERENCES

(1) Arnoldi, A.; Dallavalle, S.; Merlini, L.; Musso, L.; Farina, G.; Moretti, M.; Jayasinghe, L. Synthesis and antifungal activity of a series of N-substituted [2-(2,4-dichlorophenyl)-3-(1,2,4-triazol-1-yl)]-propylamines. *J. Agric. Food Chem.* **2007**, *55*, 8187−8192.

(2) Guillon, J.; Cohen, A.; Gueddouda, N. M.; Das, R. N.; Moreau, S.; Ronga, L.; Savrimoutou, S.; Basmaciyan, L.; Monnier, A.; Monget, M.; Rubio, S.; Garnerin, T.; Azas, N.; Mergny, J.-L.; Mullié, C.; Sonnet, P. Design, Synthesis and Antimalarial Activity of Novel Bis{N-[(Pyrrolo[1,2-a]Quinoxalin-4-Yl)Benzyl]-3-Aminopropyl} amine Derivatives. *J. Enzyme Inhib. Med. Chem.* **2017**, *32*, 547−563.

(3) Mahmud, T.; Rehman, R.; Gulzar, A.; Khalid, A.; Anwar, J.; Shafique, U.; Waheed-uz-Zaman; Salman, M. Synthesis, Characterization and Study of Antibacterial Activity of Enaminone Complexes of Zinc and Iron. *Arabian J. Chem.* **2010**, *3*, 219−224.

(4) Jensen, E. M.; Liu, O. C. Inhibitory Effect of Simple Aliphatic Amines on Influenza Virus in Tissue Culture. *Proc. Soc. Exp. Biol. Med.* **1963**, *112*, 456−459.

(5) Hotzel, C.; Marotto, A.; Pindur, U. New Propylamine Oligopyrrole Carboxamides Linked to a Heterocyclic or Anthraquinone System: Synthesis, DNA Binding, Topoisomerase I Inhibition and Cytotoxicity. *Eur. J. Med. Chem.* **2003**, *38*, 189−197.

(6) Annenkov, V. V.; Patwardhan, S. V.; Belton, D.; Danilovtseva, E. N.; Perry, C. C. A New Stepwise Synthesis of a Family of Propylamines Derived from Diatom BiffinsSilaffins and Their Activity in Silicification. *Chem. Commun.* **2006**, *14*, 1521−1523.

(7) Kabashin, A. V.; Meunier, M. Laser Ablation-Based Synthesis of Functionalized Colloidal Nanomaterials in Biocompatible Solutions. *J. Photochem. Photobiol., A* **2006**, *182*, 330−334.

(8) Sylvestre, J.-P.; Poulin, S.; Kabashin, A. V.; Sacher, E.; Meunier, M.; Luong, J. H. T.; Montre, Ä. P. De.; Postale, C. Surface Chemistry of Gold Nanoparticles Produced by Laser Ablation in Aqueous Media. *J. Phys. Chem. B* **2004**, *108*, 16864−16869.

(9) Chen, Y.; Espeel, P.; Reinicke, S.; Du Prez, F. E.; Stenzel, M. H. Control of CopolymerGlycopolymer Nanoparticle Morphology by a One-Pot, Double Modification Procedure Using TestolactonesThiolactones. *Macromol. Rapid Commun.* **2014**, *35*, 1128−1134.

(10) Woo, K.; Hong, J.; Ahn, J.-P. Synthesis and Surface Modification of Hydrophobic Magnetite to Processible Magnetite@silica-Propylamine. *J. Magn. Magn. Mater.* **2005**, *293*, 177−181.

(11) Sartori, G.; Bigi, F.; Maggi, R.; Sartorio, R.; Macquarrie, D. J.; Lenarda, M.; Storaro, L.; Coluccia, S.; Martra, G. Catalytic Activity of Aminopropyl Xerogels in the Selective Synthesis of (E)-Nitroalkenes Nitrostyrenes from NitroalkenesNitroalkanes and Aromatic Aldehydes. *J. Catal.* **2004**, *222*, 410−418.

(12) Xu, X. T.; Zhai, J. P.; Chen, Y. P.; Li, I. L.; Chen, H. Y.; Ruan, S. C.; Tang, Z. K. Synthesis of Large Single Crystals of AlPO-LTA by Using n-Propylamine as Structure Directing Agent. *J. Cryst. Growth* **2014**, *407*, 1−5.

(13) Firouzabadi, H.; Iranpoor, N.; Ghaderi, A.; Ghavami, M.; Hoseini, S. J. Palladium Nanoparticles Supported on Aminopropyl-Functionalized Clay as Efficient Catalysts for Phosphine-Free c-c Bond Formation via Mizoroki-Heck and Suzuki-Miyaura Reactions. *Bull. Chem. Soc. Jpn.* **2011**, *84*, 100−109.

(14) Ojo, A. F.; McCusker, L. B. AlPO4-Based Molecular Sieves Synthesized in the Presence of Di-n-Propylamine: Are the Structures Related? *Zeolites* **1991**, *11*, 460−465.

(15) Fouda, A. S.; Mostafa, H. A.; El-Taib, F.; Elewady, G. Y. Synergistic Influence of Iodide Ions on the Inhibition of Corrosion of C-Steel in Sulphuric Acid by Some Aliphatic Amines. *Corros. Sci.* **2005**, *47*, 1988−2004.

(16) Hassanzadeh, A. Validity of Dynamic Electrochemical Impedance Spectra of Some Amine Corrosion Inhibitors in Petroleum/Water Corrosive Mixtures by Kramers-Kronig Transformation. *Corros. Sci.* **2007**, *49*, 1895−1906.

(17) Wolfe, T. A.; Demirel, T.; Baumann, E. R. Interaction of Aliphatic Amines with Montmorillonite to Enhance Adsorption of Organic Pollutants. *Clays Clay Miner.* **1985**, *33*, 301−311.

(18) Aziz, B.; Hedin, N.; Bacsik, Z. Quantification of Chemisorption and Physisorption of Carbon Dioxide on Porous Silica Modified by Propylamines: Effect of Amine Density. *Microporous Mesoporous Mater.* **2012**, *159*, 42−49.

(19) Altarawneh, M.; Almatarneh, M. H.; Marashdeh, A.; Dlugogorski, B. Z. Decomposition of ethylamine through bimolecular reactions. *Combust. Flame* **2016**, *163*, 532−539.

(20) Dean, A. M.; Bozzelli, J. W. Combustion chemistry of nitrogen. Gardiner, W. C., Jr., Ed.; *Gas-Phase Combust. Chem.* 2000, 125−341.

DOI: 10.1021/acsomega.8b02792
ACS Omega 2019, 4, 3306−3313

(21) Almatarneh, M. H.; Elayan, I. A.; Poirier, R. A.; Altarawneh, M. The Ozonolysis of Cyclic Monoterpenes: A Computational Review. *Can. J. Chem.* **2018**, *96*, 281−292.
(22) Reiner, E. J.; Poirier, R. A.; Peterson, M. R.; Csizmadia, I. G.; Harrison, A. G. Unimolecular Fragmentation of Some Gaseous Protonated Amines. *Can. J. Chem.* **1986**, *64*, 1652−1660.
(23) Audier, H. E.; Morton, T. H. Rearrangements in metastable ion decompositions of protonated propylamines. *Org. Mass Spectrom.* **1993**, *28*, 1218−1224.
(24) Sigsby, M. L.; Day, R. J.; Cooks, R. G. Fragmentation of even electron ions: Protonated amines and esters. Org. *Org. Mass Spectrom.* **1979**, *14*, 556−561.
(25) Cho, J.; Choi, C. H. Thermal Decomposition Mechanisms of Methylamine, Ethylamine, and 1-Propylamine on Si(100)-2 × 1 Surface. *J. Chem. Phys.* **2011**, *134*, 194701.
(26) Taylor, H. A.; Achilles, H. E. The Thermal Decomposition of Propylamine. *J. Phys. Chem.* **1931**, *35*, 2658−2666.
(27) Sickman, D. V.; Rice, O. K. The Thermal Decomposition of Propylamine. *J. Am. Chem. Soc.* **1935**, *57*, 22−24.
(28) Hirota, K.; Fujita, I.; Yamamoto, M.; Niwa, Y. Electron Distribution of Electron-Bombarded Alkylamines and Its Correlation with the Probability of Bond Scission in Their Mass Spectra. *J. Phys. Chem.* **1970**, *74*, 410−415.
(29) Bodi, A.; Kercher, J. P.; Bond, C.; Meteesatien, P.; Sztáray, B.; Baer, T. Photoion Photoelectron Coincidence Spectroscopy of Primary Amines RCH_2NH_2 (R = H, CH_3, C_2H_5, C_3H_7, i-C_3H_7): Alkylamine and Alkyl Radical Heats of Formation. *J. Phys. Chem. A* **2006**, *110*, 13425−13433.
(30) Takeuchi, T.; Yamamoto, M.; Nishimoto, K. Theoretical Study on Electron Impact Mass Spectrometry. III. ab initio MO study on the Fragmentation. *J. Mass Spectrom. Soc. Jpn.* **1986**, *34*, 267−278.
(31) Bowed, R.; Maccoll, A. Low-energy, Low temperature Mass Spectra, 4-Saturated Alkylamines. *Org. Mass Spectrom.* **1985**, *20*, 331−335.
(32) Yamamoto, M.; Takeuchi, T.; Nishimoto, K. A study of low energy electron impact mass spectra using molecular orbital theory. *Int. J. Mass Spectrom. Ion Phys.* **1983**, *46*, 239−242.
(33) Upson, F. W.; Sands, L. The Decomposition of Amines in the Vapor Stage. *J. Am. Chem. Soc.* **1922**, *44*, 2306−2310.
(34) Bouchoux, G.; Salpin, J.-Y. Gas-phase basicities of polyfunctional molecules. Part 2: Saturated basic sites. *Mass Spectrom. Rev.* **2011**, *31*, 353−390.
(35) Bouchoux, G. Gas-phase basicities of polyfunctional molecules. Part 1: Theory and methods. *Mass Spectrom. Rev.* **2007**, *26*, 775−835.
(36) Gauthier, J. W.; Trautman, T. R.; Jacobson, D. B. Sustained off-resonance irradiation for CAD involving FTMS. CAD technique that emulates infrared multiphoton dissociation. *Anal. Chim. Acta* **1991**, *246*, 211−225.
(37) Moritz, F.; Grotemeyer, J. Spectroscopy and fragmentation of alkylamines investigated by photoionization. *Org. Mass Spectrom.* **1993**, *28*, 207−215.
(38) Tsuchiya, M.; Tamura, K. Study of ions with excess kinetic energy. III—Mass spectra of excess kinetic energy ions of aliphatic amines. *Org. Mass Spectrom.* **1976**, *11*, 1281−1289.
(39) Frisch, M. J.; Trucks, G. W.; Schlegel, H. B.; Scuseria, G. E.; Robb, M. A.; Cheeseman, J. R.; Scalmani, G.; Barone, V.; Mennucci, B.; Petersson, G. A.; et al. *Gaussian 09*, Revision A.02; Gaussian, Inc.: Wallingford, CT, 2009.
(40) Becke, A. D. Density-functional thermochemistry. III. The role of exact exchange. *J. Chem. Phys.* **1993**, *98*, 5648−5652.
(41) Lee, C.; Yang, W.; Parr, R. G. Development of the CalleColle-SalvedSalvetti Correlation-Energy Formula into a Functional of the Electron Density. *Phys. Rev. B: Condens. Matter Mater. Phys.* **1988**, *37*, 785−789.
(42) Hehre, W. J.; Ditchfield, R.; Pople, J. A. Self-consistent molecular orbital methods. XII. Further extensions of Gaussian-type basis sets for use in molecular orbital studies of organic molecules. *J. Chem. Phys.* **1972**, *56*, 2257−2261.
(43) Montgomery, J. A.; Frisch, M. J.; Ochterski, J. W.; Petersson, G. A. A complete basis set model chemistry. VII. Use of the minimum population localization method. *J. Chem. Phys.* **2000**, *112*, 6532−6542.
(44) Almatarneh, M. H.; Altarawneh, M.; Poirier, R. A.; Saraireh, I. A. High level ab initio, DFT, and RRKM calculations for the unimolecular decomposition reaction of ethylamine. *J. Comput. Sci.* **2014**, *5*, 568−575.
(45) Almatarneh, M. H.; Barhoumi, L.; Al-Tayyem, B.; Abu-Saleh, A. A.-A. A.; AL-A'qarbeh, M. M.; Abuorabi, F.; AlShamaileh, E.; Altarawneh, M.; Marashdeh, A. Computational Study for the Second-Stage Cracking of the Pyrolysis of Ethylamine: Decomposition of MethenamineMethanimine, MethenamineEthenamine, and EthanediamineEthanimine. *Comput. Theor. Chem.* **2016**, *1075*, 9−17.
(46) Altarawneh, M.; Al-Muhtaseb, A. a. H.; Almatarneh, M. H.; Poirier, R. A.; Assaf, N. W.; Altarawneh, K. K. Theoretical Investigation into Competing Unimolecular Reactions Encountered in the Pyrolysis of Acetamide. *J. Phys. Chem. A* **2011**, *115*, 14092−14099.
(47) Al-Muhtaseb, A. a. H.; Altarawneh, M.; Almatarneh, M. H.; Poirier, R. A.; Assaf, N. W. Theoretical study on the unimolecular decomposition of thiophenol. *J. Comput. Chem.* **2011**, *32*, 2708−2715.
(48) Fukui, K. The path of chemical reactions - the IRC approach. *Acc. Chem. Res.* **1981**, *14*, 363−368.

DOI: 10.1021/acsomega.8b02792
ACS Omega 2019, 4, 3306−3313